Inorganic Chemistry

Article

pubs.acs.org/IC

New Lithium Copper Borates with BO_3 Triangles: $Li_6CuB_4O_{10}$, $Li_3CuB_3O_7$, $Li_8Cu_7B_{14}O_{32}$, and $Li_2Cu_9B_{12}O_{28}$

N. V. Kuratieva,[†,‡] M. Bànki,[‡] A. A. Tsirlin,[§,∥] J. Eckert,[‡,⊥] H. Ehrenberg,[‡,#] and D. Mikhailova*[,‡,§]

[†]Institute of Inorganic Chemistry SB, Russian Academy of Sciences, Acad. Lavrentiev Avenue 3, Novosibirsk 630090, Russia

[‡]Institute for Complex Materials, IFW Dresden, P.O. Box 27 01 16, D-01171 Dresden, Germany

[§]Max Planck Institute for Chemical Physics of Solids, Nöthnitzer Str. 40, D-01187 Dresden, Germany

[∥]National Institute of Chemical Physics and Biophysics, Akadeemia tee 23, 12618 Tallinn, Estonia

[⊥]Institute of Materials Science, TU Dresden, D-01062 Dresden, Germany

[#]Institute for Applied Materials (IAM), Karlsruhe Institute of Technology (KIT), Hermann-von-Helmholtz-Platz 1, 76344 Eggenstein-Leopoldshafen, Germany

Supporting Information

ABSTRACT: Crystal structures of three new lithium copper borates, $Li_3CuB_3O_7$, $Li_8Cu_7B_{14}O_{32}$, and $Li_2Cu_9B_{12}O_{28}$, and a new $Li_6CuB_4O_{10}$ polymorph were solved by single-crystal X-ray diffraction. In all of the structures, the boron cations form BO_3 triangles, which are connected with each other and with copper polyhedra only via corners in $Li_6CuB_4O_{10}$ and $Li_3CuB_3O_7$ and via both corners and edges in $Li_8Cu_7B_{14}O_{32}$ and $Li_2Cu_9B_{12}O_{28}$. The $Li_3CuB_3O_7$ and $Li_8Cu_7B_{14}O_{32}$ compounds were synthesized as pure samples with only trace amounts of impurities; hence, their magnetic properties could be investigated and analyzed in terms of underlying magnetic couplings. Other compositions always represented multiphase mixtures. $Li_3CuB_3O_7$ features infinite Cu,O chains formed by Cu_2O_6 units consisting of edge-shared CuO_4 squares. Together with two apical oxygen atoms with long interatomic Cu−O distances of 2.7−2.8 Å, the Cu_2O_6 units form chains extended along the *a* axis. These pseudochains are responsible for strong anisotropic thermal expansion behavior. The temperature dependence of the magnetization between 4 and 380 K for $Li_3CuB_3O_7$ could be fit well by a spin-dimer model. The magnetic susceptibility of $Li_8Cu_7B_{14}O_{32}$ showed a more complex temperature dependence, with two different Curie−Weiss regimes in the temperature range of 2−380 K.

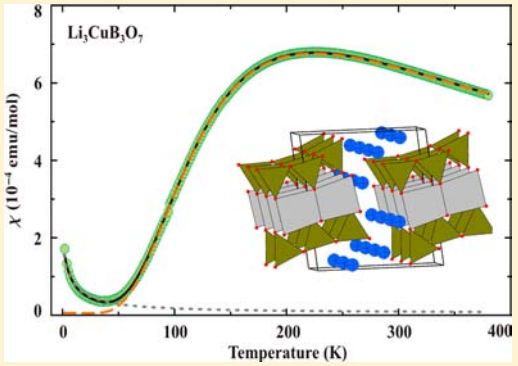

INTRODUCTION

Copper-containing borates have attracted interest as inorganic compounds with intricate crystal structures and diverse physical properties.[1−5] The Jahn−Teller distortion of Cu^{2+} (d^9 electronic configuration) often leads to a low-dimensional character of the crystal structure and to a strong anisotropy of physical properties. Recently, copper borates have been investigated as (*i*) potential optical materials (both crystalline phases[1] and glasses[2]), (*ii*) magnetic materials with unusual low-temperature behavior,[3,4] (*iii*) photocatalysts,[5] and (*iv*) electrode materials for lithium-ion batteries.[6,7]

The strong Jahn−Teller effect of Cu^{2+} distinguishes copper borates from other borates with divalent transition metals. For example, $Co_3(BO_3)_2$ and $Ni_3(BO_3)_2$ form three-dimensional networks containing separate BO_3 triangles and practically undistorted MO_6 octahedra,[8] while $Cu_3(BO_3)_2$ features a layered structure with separate CuO_4 polyhedra that share corners with each other or with BO_3 groups.[9] In most known copper-containing borates, boron cations form planar BO_3 triangles, although some structures exhibit both BO_3 triangles and BO_4 tetrahedra, as in another $Cu_3(BO_3)_2$ polymorph with a pseudolayered monoclinic structure[10] or in $MCuB_7O_{12}{\cdot}nH_2O$ (M = Na, K) with a framework formed by octahedral CuO_6, tetrahedral BO_4, and triangular BO_3 units.[11] The crystal structure of CuB_2O_4 contains only corner-sharing BO_4 tetrahedra.[12] High-pressure conditions seem to stabilize BO_4 tetrahedra and eliminate structural differences between double transition metal borates: the high-pressure modification of CuB_4O_7 contains only BO_4 tetrahedra. It is isostructural with MB_4O_7 (M = Ni, Mn, Zn).[13]

Since quite different structure types were found for double copper borates and for borates of other transition metals under normal conditions, a similar situation could be expected for ternary borates, such as lithium copper borates, which may be suitable materials for intercalation of lithium cations. However, despite numerous investigations of $LiM(II)BO_3$ phases (M = Fe, Co, Mn), information about compounds in the Li−Cu−B−O system is very scarce.[1,14,15] Three compounds with the supposed $Li_4CuB_2O_6$, $Li_2Cu_2B_2O_6$, and $Li_2CuB_4O_8$ stoichiom-

Received: June 27, 2013
Published: November 22, 2013

   dx.doi.org/10.1021/ic4015724 | Inorg. Chem. 2013, 52, 13974−13983

Table 1. Details of Single-Crystal X-ray Data Collection and Structure Refinement of Lithium Copper Borates

Crystal Data				
chemical formula	$Li_3CuB_3O_7$	$Li_2Cu_9B_{12}O_{28}$	$Li_8Cu_7B_{14}O_{32}$	$Li_6CuB_4O_{10}$
formula weight	228.80	1163.46	1163.64	308.42
crystal system	triclinic	triclinic	orthorhombic	triclinic
space group	$P\bar{1}$	$P\bar{1}$	$Pca2_1$	$P\bar{1}$
a (Å)	3.313(2)	3.2984(8)	25.447(10)	3.2882(12)
b (Å)	8.756(5)	9.857(3)	3.3185(13)	6.645(3)
c (Å)	9.485(6)	16.152(4)	14.200(6)	9.196(3)
α (deg)	84.59(5)	94.333(5)		78.865(13)
β (deg)	88.70(5)	95.383(5)		89.757(14)
γ (deg)	85.06(5)	96.494(5)		86.556(13)
cell volume (Å^3)	272.9(3)	517.5(2)	1199.1(8)	196.79(13)
Z	2	1	2	1
D_{calcd} (g/cm^3)	2.785	3.733	3.223	2.603
radiation type	Mo Kα, λ = 0.71073 Å			
T (K)	296(2)	296(2)	296(2)	296(2)
crystal form, color	prism, blue	prism, turquoise	prism, light blue	prism, light blue
crystal size (mm^3)	0.10 × 0.09 × 0.04	0.34 × 0.20 × 0.20	0.06 × 0.03 × 0.03	0.10 × 0.06 × 0.04
Data Collection				
diffractometer	Oxford Diffraction Xcalibur single-crystal X-ray diffractometer with sapphire CCD detector	Bruker Kappa Apex II single-crystal X-ray diffractometer with CCD detector		
data collection method	rotation method with data acquisition using ω and φ scan(s)			
absorption coefficient (mm^{-1})	3.983	9.201	6.240	2.818
F(000)	218	551	1106	147
θ range for data collection (deg)	2.16−28.75	1.27−27.48	1.6−26.36	2.26−27.65
h, k, l ranges	$-4 \le h \le 4$ $-11 \le k \le 10$ $-12 \le l \le 12$	$-4 \le h \le 4$ $-10 \le k \le 12$ $-17 \le l \le 20$	$-29 \le h \le 31$ $-4 \le k \le 2$ $-17 \le l \le 14$	$-4 \le h \le 3$ $-7 \le k \le 8$ $-6 \le l \le 12$
reflns collected/unique [R_{int}]	4549/1342 [0.0261]	3514/2343 [0.0133]	7022/2298 [0.0505]	1383/875 [0.0184]
completeness to θ = 25.00°	99.9	98.9	99.5	96.9
refinement method	full-matrix least-squares on F^2			
data/restraints/parameters	1342/0/127	2343/0/226	2298/1/245	875/0/97
goodness of fit on F^2	1.043	1.061	1.063	1.148
R_1, wR_2 [$I > 2\sigma(I)$]	0.0264, 0.0420	0.0408, 0.1143	0.0362, 0.0741	0.0234, 0.0570
Flack parameter	−	−	0.45(3)	−
R_1, wR_2 (all data)	0.0404, 0.0442	0.0471, 0.1178	0.0476, 0.0776	0.0251, 0.0578
largest diff. peak/hole (e/Å^3)	0.425/−0.429	1.500/−1.479	0.685/−1.001	0.367/−0.348

etry were found during investigations of this ternary phase diagram at about 1273 K in air,[14] but neither crystal structures nor cell parameters were reported. On the basis of IR measurements, the presence of BO_3 triangles in $Li_4CuB_2O_6$ and $Li_2CuB_4O_8$ and both BO_3 triangles and BO_4 tetrahedra in $Li_2Cu_2B_2O_6$ has been conjectured.[14] Another lithium copper borate, $Li_6CuB_4O_{10}$, is obtained at significantly lower temperatures and exhibits isolated $[CuB_4O_{10}]^{6-}$ units. It is a nonlinear optical material[1] and presumably undergoes temperature-induced phase transitions.[15]

In the present work, the three new compounds $Li_3CuB_3O_7$, $Li_2Cu_9B_{12}O_{28}$, and $Li_8Cu_7B_{14}O_{32}$ as well as a new polymorph of $Li_6CuB_4O_{10}$ were identified by single-crystal X-ray diffraction after annealing of several compositions from the Li_2O−CuO−B_2O_3 system at 1273 K in air. The unusual magnetic properties of $Li_3CuB_3O_7$ and $Li_8Cu_7B_{14}O_{32}$ together with the strongly anisotropic thermal expansion of $Li_3CuB_3O_7$ could be explained through the pronounced low-dimensional character of the crystal structures. This low dimensionality is related to the Jahn−Teller distortion of copper−oxygen polyhedra, similar to that in double copper borates.

EXPERIMENTAL SECTION

Syntheses. Polycrystalline $Li_3CuB_3O_7$ and $Li_8Cu_7B_{14}O_{32}$ powders were synthesized from stoichiometric amounts of Li_2CO_3 (Alfa Aesar, 99.9%), CuB_2O_4, and H_3BO_3 (Alfa Aesar, 99.99%) in air in platinum crucibles at 1273 K during slow cooling (10−15 K/h) of the melt. CuB_2O_4 was obtained from a mixture of CuO (Alfa Aesar, 99.95%) and H_3BO_3, taken in stoichiometric amounts, in air at 1273 K after annealing for 70 h with intermediate grinding. Single crystals of $Li_3CuB_3O_7$ were recovered after melting the samples with the compositions "$Li_2CuB_2O_5$" and "$Li_2CuB_4O_8$" at 1373 K in air over 50 h and furnace-cooling them to room temperature. Single crystals of $Li_2Cu_9B_{12}O_{28}$, $Li_8Cu_7B_{14}O_{32}$, and a new polymorph of $Li_6CuB_4O_{10}$ were obtained by melting the sample with the "$Li_2Cu_2B_2O_6$" stoichiometry at 1298 K over 50 h in air and furnace-cooling it to room temperature. All of these samples were solidified melts and contained multiple phases. The compositions $Li_2CuB_4O_8$ and $Li_2Cu_2B_2O_6$ were proposed in the work[14] as individual compounds.

Phase Analysis. Phase analysis and determination of the cell parameters of $Li_3CuB_3O_7$ and $Li_8Cu_7B_{14}O_{32}$ at room temperature and

dx.doi.org/10.1021/ic4015724 | Inorg. Chem. 2013, 52, 13974−13983

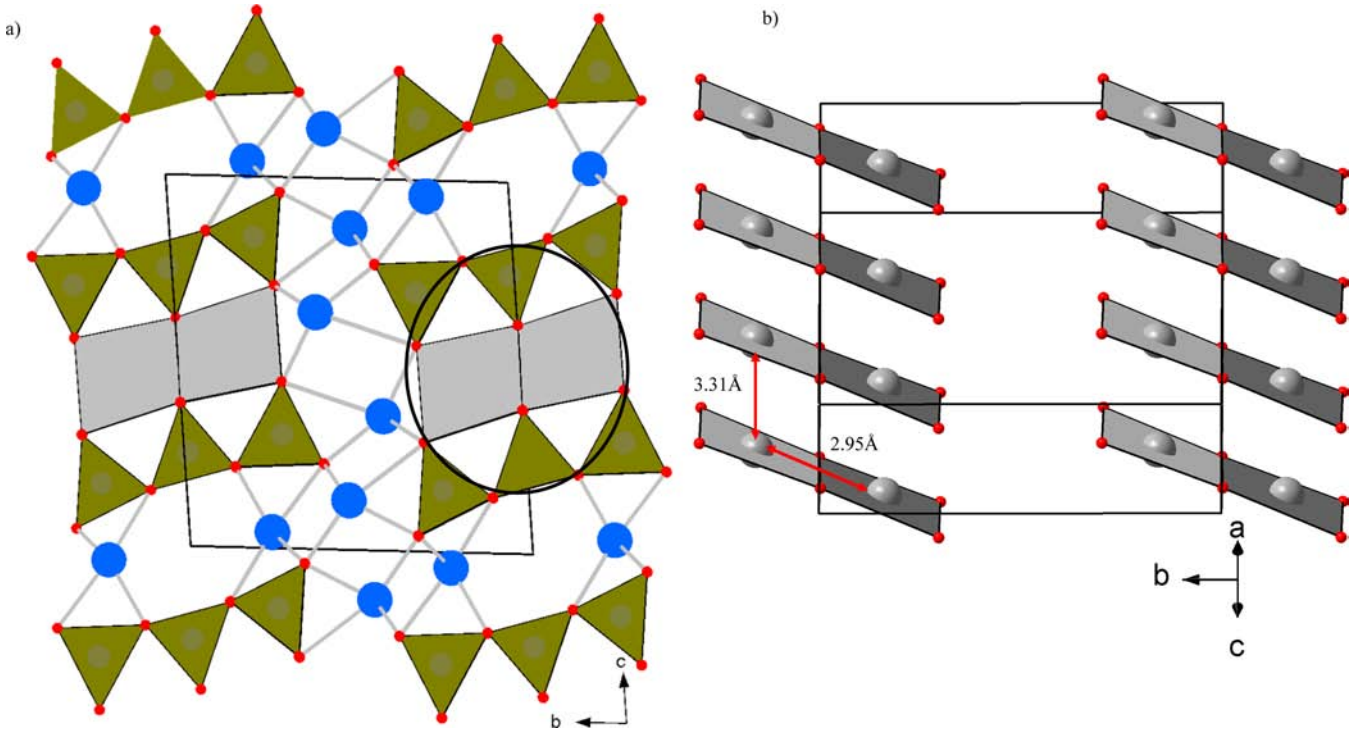

Figure 1. (a) Crystal structure of $Li_3CuB_3O_7$ in the *bc* plane and (b) Cu_2O_6 units in the *ab* plane (b). In (a), blue spheres represent Li atoms and gray polyhedra represent Cu_2O_6 units.

high-temperature structure investigations of $Li_3CuB_3O_7$ at up to 1000 K were carried out using powder X-ray diffraction (PXRD) with a STOE STADI P diffractometer (Mo Kα_1 radiation, λ = 0.7093 Å) in transmission mode. According to the PXRD results, the $Li_3CuB_3O_7$ samples contained 95% (w/w) desired compound and about 5% (w/w) $LiBO_2$ as a second phase, whereas 5% CuO was present in the $Li_8Cu_7B_{14}O_{32}$ samples together with 95% main phase.

Crystal Structures. The crystal structure of $Li_3CuB_3O_7$ was solved at 295 K by single-crystal X-ray diffraction using the Xcalibur system from Oxford Diffraction. The software package SHELXTL[16] as included in X-STEP32[17] was used for structure solution and refinement. A combined empirical absorption correction with frame scaling was applied using the SCALE3 ABSPACK command in CrysAlis Red.[18]

Single-crystal X-ray diffraction data for $Li_2Cu_9B_{12}O_{28}$, $Li_8Cu_7B_{14}O_{32}$, and a new polymorph of $Li_6CuB_4O_{10}$ were collected using graphite-monochromatized Mo Kα radiation (λ = 0.71073 Å) at 296 K on a Bruker Kappa Apex II CCD diffractometer equipped with a 4 K CCD area detector. The φ-scan technique was employed to measure intensities. Absorption corrections were applied using the SADABS program.[19] The crystal structures were solved by direct methods and refined by full-matrix least-squares techniques with the use of the SHELXTL package.[16] All of the atomic thermal displacement parameters were refined anisotropically.

Magnetization Measurements. The magnetizations of $Li_3CuB_3O_7$ and $Li_8Cu_7B_{14}O_{32}$ were measured with a superconducting quantum interference device (SQUID) from Quantum Design. Measurements were done in the field-cooled and zero-field-cooled modes over the temperature range from 1.8 to 380 K with external magnetic field strengths of 0.5−5 T.

Electronic Structure Calculations. The electronic structure of $Li_3CuB_3O_7$ was calculated within the framework of density functional theory (DFT) using the FPLO code[20] and the local density approximation (LDA) exchange−correlation potential.[21] Magnetic couplings were obtained by mapping the LDA band structure onto a tight-binding model and, subsequently, onto a Hubbard model or from energy differences between the ferromagnetic and antiferromagnetic spin configurations calculated within the LSDA+*U* approach, where *U* = 6 eV[22] implies the mean-field correction for correlation effects in the Cu 3d shell, and additionally, an on-site Hund's exchange of *J* = 1 eV was introduced into the self-consistent procedure. A comprehensive description of the computational method can be found in refs 22−24.

RESULTS AND DISCUSSION

1. Crystal Structures. To explore the Li_2O−CuO−B_2O_3 system, we repeated the syntheses of $Li_2CuB_4O_8$ and $Li_2Cu_2B_2O_6$ as reported in ref 14 and additionally prepared samples with the "$Li_2CuB_2O_5$" stoichiometry, which is similar to $Li_2MgB_2O_5$.[25] Different blue and green crystals together with black crystals of CuO and white crystals of several lithium boron oxides were found. Four new lithium−copper borates were identified (Table 1). Atomic coordinates and equivalent isotropic displacement parameters (Ueq) for the lithium copper borates are presented in Tables A−D in the Supporting Information. U_{eq} was defined as one-third of the trace of the orthogonalized U^{ij} tensor. In all of the compounds, boron adopts a triangular oxygen coordination. Copper atoms are surrounded by distorted octahedra, pyramids, and squares of oxygen atoms. Mixed Li/Cu occupancy was observed in $Li_8Cu_7B_{14}O_{32}$.

1.1. $Li_3CuB_3O_7$. Annealing of the "$Li_2CuB_2O_5$" samples at 1273 K for 50 h led to a mixture of $LiBO_2$,[26] CuO, and an unknown phase. Single-crystal studies of the light-blue crystals revealed their triclinic symmetry and $Li_3CuB_3O_7$ stoichiometry (see Table 1 in the text and the tables in the Supporting Information). The same composition, $Li_3MB_3O_7$, was described during a phase search in the Li_2O−ZnO−B_2O_3 system. The zinc-containing compound probably crystallizes in an orthorhombic symmetry, but detailed structural information was not reported.[27]

The structure of $Li_3CuB_3O_7$ contains nearly planar, isolated binuclear anions $[Cu_2(B_3O_7)_2]^{6-}$ (Figure 1), allowing a chemical formula of $Li_6Cu_2B_6O_{14}$ or $Li_6[Cu_2(B_3O_7)_2]$ to be

dx.doi.org/10.1021/ic4015724 | *Inorg. Chem.* 2013, 52, 13974−13983

introduced. The triborate anion consists of three corner-sharing BO_3 triangles with the triangular planes slightly twisted by 9.2 and 9.8°. The maximum deviations from the mean plane of the triborate anion are seen for the terminal oxygen atoms O(4) and O(7), which are offset by 0.133 and 0.123 Å, respectively, compared with the mean deviation of 0.073 Å. Two triborate anions share six O atoms with Cu atoms to form the binuclear complex anions $[Cu_2(B_3O_7)_2]^{6-}$.

In order to define unambiguously the coordination polyhedra for the copper ions, bond-valence sum calculations with the bond-valence parameters R_0 = 1.679 Å and B = 0.370 Å[28−30] were performed assuming a copper oxidation state of +2 and an oxygen oxidation state of −2. For the $Li_3CuB_3O_7$ compound, the bond-valence sum calculations revealed CuO_4 squares as the coordination polyhedra, with Cu−O distances of about 1.92 Å. Together with two apical oxygen atoms with Cu−O interatomic distances of 2.665(3) and 2.783(3) Å, the Cu_2O_6 units form chains running along the a axis (Figure 1b).

Three independent Li sites are present in the structure. Li^+ ions form distorted tetrahedra and trigonal pyramids with Li−O distances in the range of 1.935−2.19 Å. The average B−O interatomic distances of 1.36−1.38 Å in the triangles are in good agreement with the B−O distances in BO_3 units in both hydrogen-free copper borate polymorphs of $Cu_3B_2O_6$.[9,10] Our single-crystal diffraction data do not give any indications of hydrogen atoms in the structure.

The temperature evolution of the crystal structure was studied by PXRD on a powder sample prepared by high-temperature annealing at 1273 K. The diffraction pattern of $Li_3CuB_3O_7$ at room temperature is presented in Figure 2.

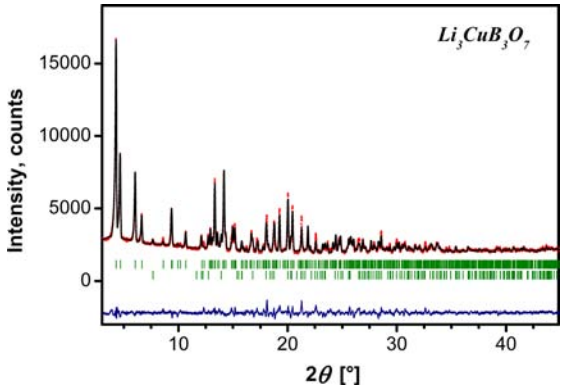

Figure 2. Observed and fitted PXRD profiles (Mo Kα_1) for $Li_3CuB_3O_7$ together with the corresponding difference curve. The fitted profiles belong to the phases $Li_3CuB_3O_7$ and $LiBO_2$[26] (from top to bottom).

Thermal expansion of $Li_3CuB_3O_7$ is highly anisotropic with a large expansion along the a axis (Figure 3) that corresponds to the increase in the largest Cu−O distance in the distorted CuO_6 octahedra.

1.2. $Li_2Cu_9B_{12}O_{28}$. The crystal structure of $Li_2Cu_9B_{12}O_{28}$ consists of chains formed by CuO_x polyhedra (Figure 4). The copper polyhedra within the chains are connected with each other via corners and edges (see Figure 4b). Two different borate groups, the diborate anion $[B_2O_5]^{4-}$ and tetraborate anion $[B_4O_9]^{2-}$, are present in the structure. The B_4O_9 groups have an open-chain structure with a small deviation from the planar configuration and radial winging (Figure 4). There are six independent positions of Cu atoms. The bond-valence sum

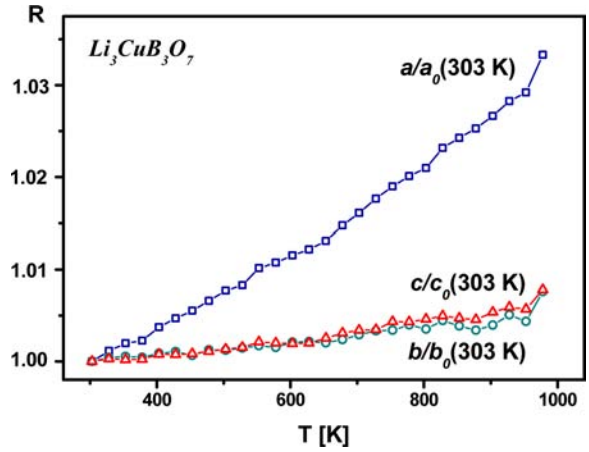

Figure 3. Relative changes in the lattice parameters a, b, and c of $Li_3CuB_3O_7$ (normalized to their values at 303 K) vs temperature. The compound melts at about 1000 K.

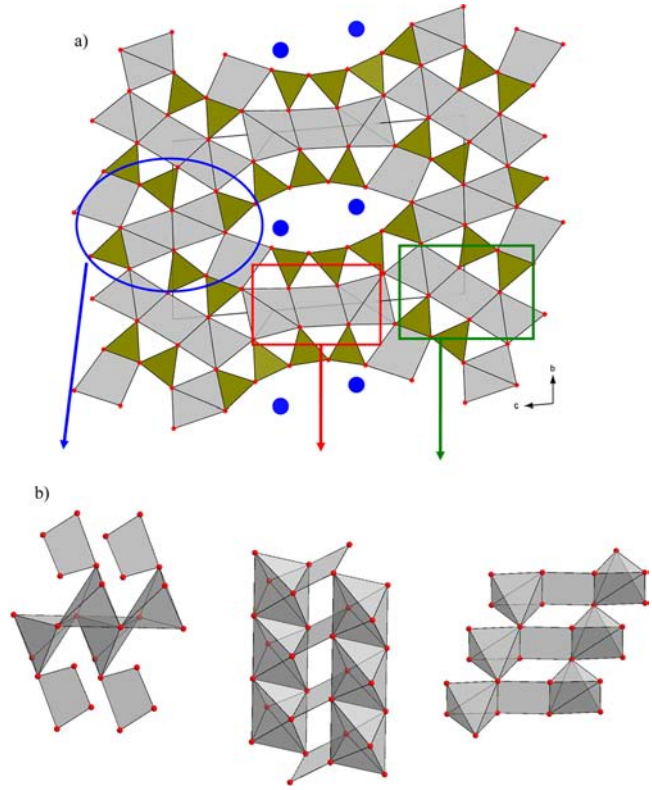

Figure 4. (a) Crystal structure of $Li_2Cu_9B_{12}O_{28}$ along the a axis and (b) the linkage of copper polyhedra in the chains. According to the bond-valence sum calculations, CuO_6 octahedra, CuO_5 square pyramids, and CuO_4 squares can be distinguished in the structure. Blue spheres represent lithium ions.

calculations for copper(II) ions led to the conclusion that the coordination polyhedra of copper are squares, square pyramids with four short and one long Cu−O distances (4 + 1), and distorted octahedra with four short and two long distances (4 + 2). The lithium atoms occupy large cavities positioned along the a axis. The only independent Li atom has a deformed polyhedron, with four short Li−O bonds between 1.94 and 2.18 Å and a longer bond of 2.38 Å. The average B−O distances of 1.36−1.38 Å are similar to the values seen in the $Cu_3B_2O_6$ structures.

dx.doi.org/10.1021/ic4015724 | Inorg. Chem. 2013, 52, 13974−13983

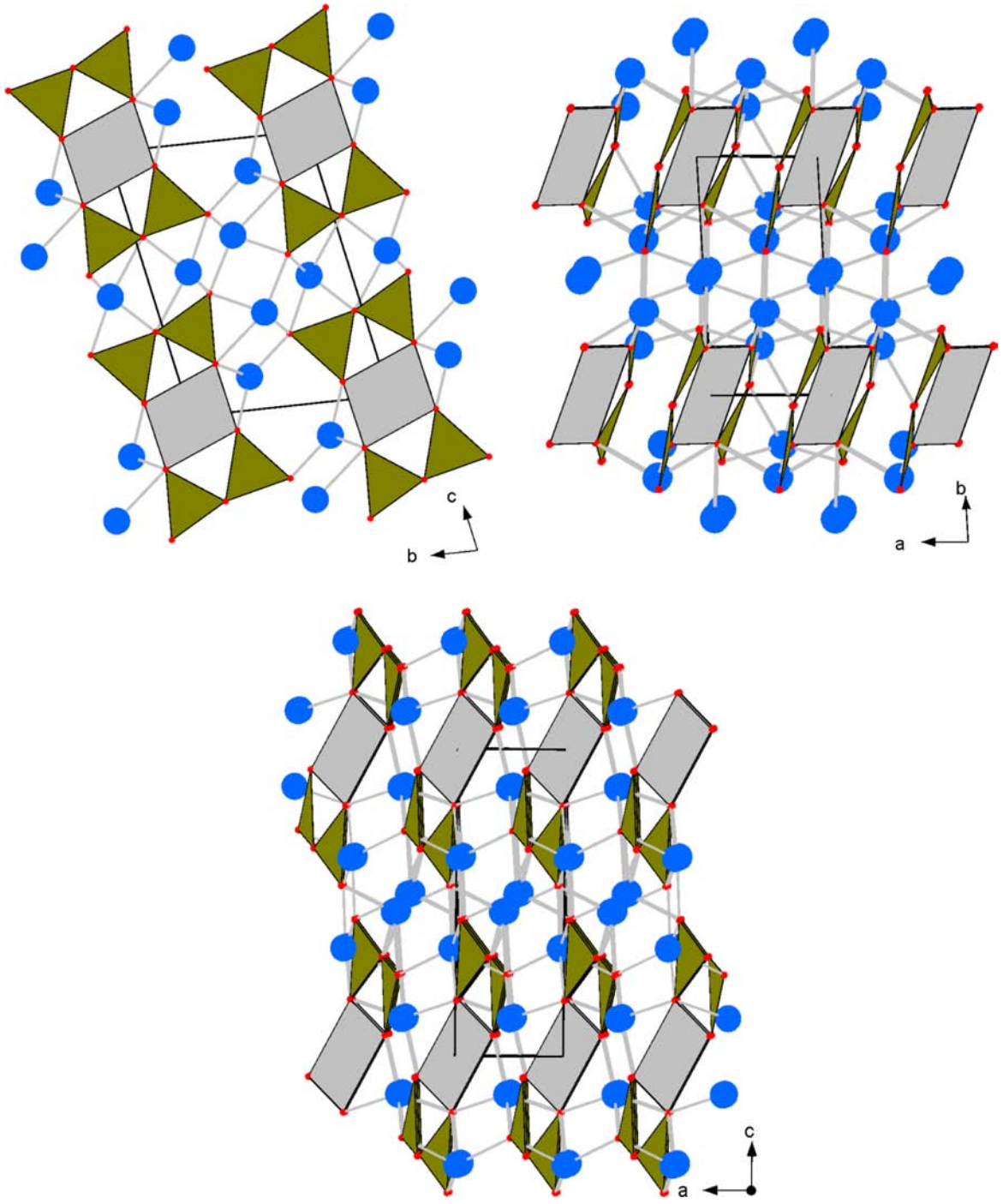

Figure 5. Crystal structure of $Li_6CuB_4O_{10}$ viewed from different directions.

It should be noted that two of the six copper sites, Cu(5) and Cu(6), are only partially occupied. These sites could be either fully occupied by Li and Cu simultaneously or partially occupied by copper atoms only. However, full occupancy of the Cu(5) and Cu(6) sites with both 0.5Li and 0.5Cu, giving the composition $Li_4Cu_8B_{12}O_{28}$, resulted in unreasonably large residuals, R_1 = 0.0832 for 2081 reflections with $I > 2\sigma(I)$, in comparison with R_1 = 0.0408 after the refinement with partial copper occupancy of these sites. Therefore, the partial occupancy of Cu should be inferred.

It should also be noted that we found elongated thermal ellipsoids for all of the oxygen atoms in the $Li_2Cu_9B_{12}O_{28}$ structure. The ellipsoids are elongated along the direction perpendicular to the structural layers. The origin of this effect is presently unclear. For example, partial occupation of the Cu(5) and Cu(6) sites might lead to a local order that is not visible in conventional single-crystal experiments.

1.3. $Li_6CuB_4O_{10}$. A new polymorph of $Li_6CuB_4O_{10}$ was identified after the synthesis of the sample with the "$Li_4CuB_2O_6$" stoichiometry. The structure of this polymorph contains discrete centrosymmetric $[Cu(B_2O_5)_2]^{6-}$ anions separated by lithium ions (Figure 5). The copper atom is located at the inversion center and is surrounded by a nearly planar square of oxygen atoms with bond lengths of 1.937(2)

dx.doi.org/10.1021/ic4015724 | *Inorg. Chem.* 2013, 52, 13974−13983

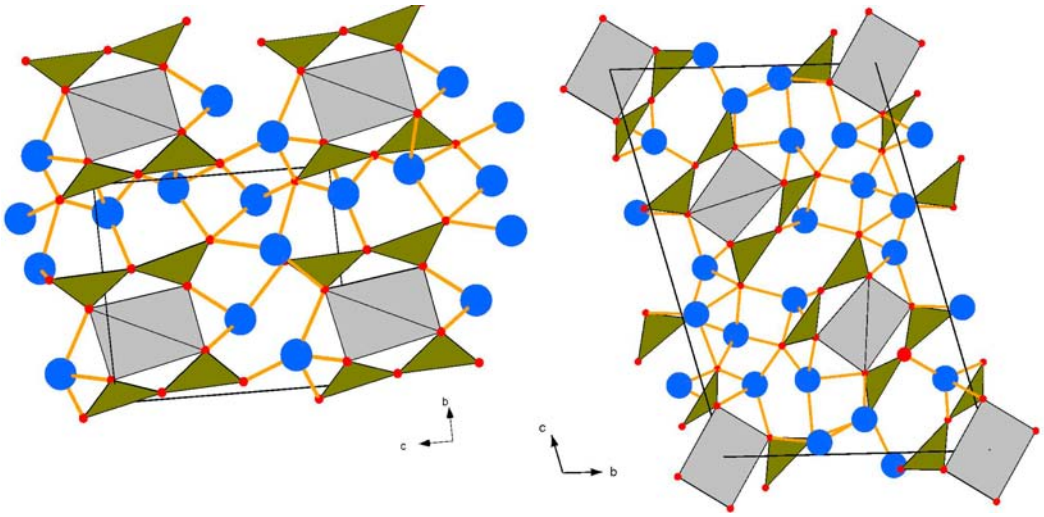

Figure 6. Crystal structures of previously known $Li_6CuB_4O_{10}$ polymorphs. The left panel shows the polymorph with the small non-centrosymmetric unit cell.[1] The right panel shows the polymorph with the 3-fold unit cell.[15] Blue spheres represent Li atoms, and gray polyhedra represent CuO_4 squares.

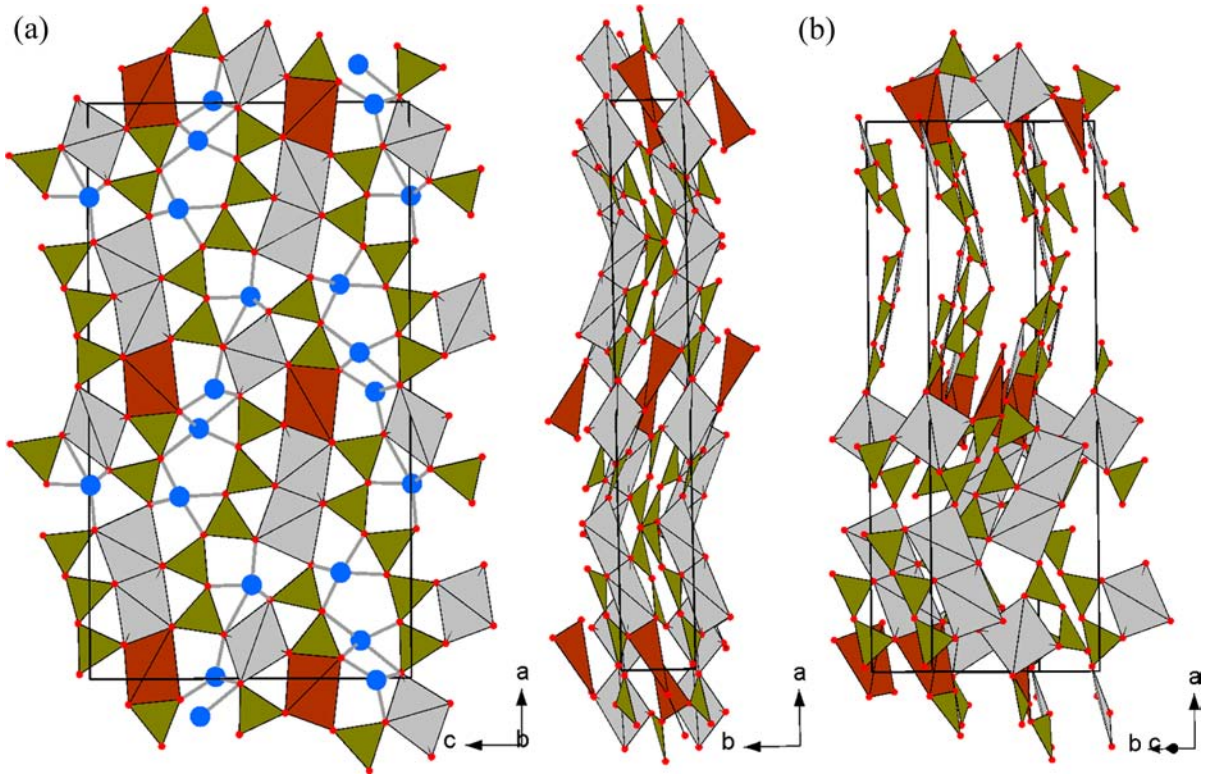

Figure 7. (a) Crystal structure of $Li_8Cu_7B_{14}O_{32}$ in the (left) *ac* plane and (right) *ab* plane without Li^+ ions. Gray polyhedra are occupied only by copper ions, whereas the brown ones are occupied by both copper and lithium ions (50%/50%). Blue spheres represent lithium ions. (b) Structural fragment of $Li_8Cu_7B_{14}O_{32}$ without Li^+ ions, showing a change in the orientation of layered segments from BO_3 triangles to CuO_4 squares along the *a* axis.

and 1.942 (2) Å. Each CuO_4 polyhedron is enclosed by two B_2O_5 units, each formed by two corner-sharing BO_3 triangles. The O−Cu−O angle adjacent to these B_2O_5 units is slightly larger than the outer O−Cu−O angle, causing the CuO_4 squares to be squeezed. Two long Cu−O contacts of 2.726(17) Å are found in the axial positions perpendicular to the CuO_4 squares. The planar $[Cu(B_2O_5)_2]^{6-}$ anions are parallel to each other. The shortest contact between the copper atoms is about 3.29 Å and corresponds to the lattice translation along *a*. The average B−O distances in the BO_3 units are 1.36−1.37 Å. The lithium atoms have tetrahedral or trigonal-bipyramidal coordination environments with bond lengths ranging between 1.872(4) Å and 2.368(5) Å.

Two other polymorphs of $Li_6CuB_4O_{10}$ have been reported.[1,15] In general, all three polymorphs represent very similar structure designs with same coordination polyhedra of copper and boron (see Figure 6). Small shifts of oxygen atoms either eliminate the inversion center and reduce the lattice

dx.doi.org/10.1021/ic4015724 | *Inorg. Chem.* 2013, 52, 13974−13983

symmetry to $P1$[1] or trigger the formation of an isosymmetric superstructure with the 3-fold unit cell volume.[15] Three structural phase transitions, two reversible and one presumably irreversible, were detected for $Li_6CuB_4O_{10}$ with the 3-fold unit cell volume from room temperature up to the melting point at 1123 K, using differential scanning calorimetry and high-temperature PXRD.[15] More detailed information about these high-temperature polymorphs is missing, however.

1.4. $Li_8Cu_7B_{14}O_{32}$. On the basis of the similar ionic radii[31] of Cu^{2+} (0.57 Å for CuO_4 tetrahedra and 0.73 Å for CuO_6 octahedra) and Li^+ (0.59 Å for LiO_4 tetrahedra and 0.76 Å for LiO_6 octahedra), the simultaneous presence of Li and Cu atoms on the same crystallographic site could be generally expected. Indeed, this mixed occupancy was observed in the new compound $Li_8Cu_7B_{14}O_{32}$.

In contrast to other the Cu^{2+} borates reported here, $Li_8Cu_7B_{14}O_{32}$ is orthorhombic. Reflection conditions indicated the presence of two glide planes, resulting in the space group *Pbcm* or its non-centrosymmetric subgroup $Pca2_1$. The refinement in *Pbcm* was ultimately unsuccessful, and even a satisfactory model could not be found with direct methods. In contrast, we were able to obtain a plausible structure solution in $Pca2_1$. The subsequent refinement of the Flack parameter resulted in the value of 0.45, indicating the racemic nature of our crystals. The structure of $Li_8Cu_7B_{14}O_{32}$ is non-centrosymmetric, as verified by the search for missing symmetry elements with the Platon software.[32]

The structure consists of nearly planar copper borate fragments that are connected to each other to form a three-dimensional framework (Figure 7). The copper atoms have square oxygen coordination with an average Cu−O distance of 1.96(4) Å. The $(Cu,Li)O_4$ polyhedron is intermediate between a tetrahedron and a square. This polyhedron is attached to the dimer formed by two CuO_4 squares (Figure 7b). Unconstrained refinement of the occupancy numbers for the mixed Cu/Li site led to a value of $^1/_2$ for each cation type. Although the refined occupancy number for Li(1) revealed a slight Li deficiency, the occupancy of this site was fixed to $^1/_2$ according to the charge balance. There are two types of borate anions, namely, diborates and pentaborates. The BO_3 triangles (with average B−O distances of 1.36−1.37 Å) in the open-chain pentaborate switch the direction in the middle of the anion, with the biggest angle value of 25.7° between the planes of BO_3 triangles (the rest of the angles are in the range of 1.7−12.2°). The lithium atoms form tetrahedra and distorted tetragonal pyramids with an average Li−O distance of 2.0(1) Å.

1.5. Implications for Lithium Transport and Intercalation. Mixed lithium copper borates with copper(II) could have an enhanced lithium conductivity and be used as intercalation materials for Li batteries. While electrochemical tests remain challenging and require suitable processing of these insulating compounds, a simple crystallographic assessment is a natural first step in choosing systems that support the transport of Li^+ ions and/or the intercalation of additional Li atoms. To this end, we analyzed the polyhedra of lithium and their connectivity.

The crystal structure of $Li_3CuB_3O_7$ exhibits channels along the *a* axis formed by BO_3 triangles and LiO_5 polyhedra (see Figure 8). These channels exhibit large voids that might be suitable for an insertion of 0.5 Li per formula unit on the 1*a* (0, 0, 0) site with full occupancy. The presence of empty channels with vacant positions suitable for Li atoms should trigger ionic transport in $Li_3CuB_3O_7$. This mechanism of diffusion resembles

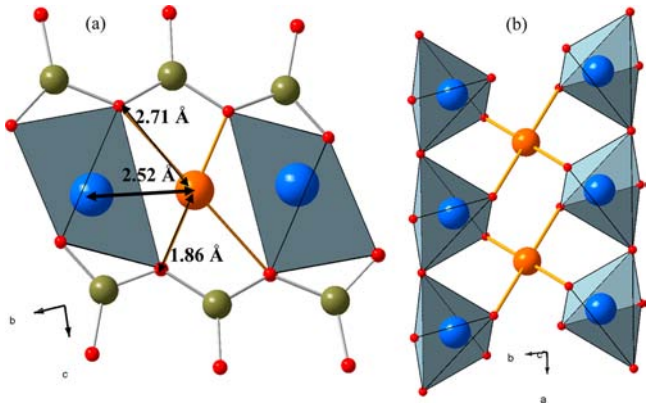

Figure 8. Structure fragments along the *a* axis in $Li_3CuB_3O_7$. Green spheres represent B atoms, blue spheres represent lithium atoms in pristine structures, and orange spheres show most likely lithium positions in the case of possible Li insertion. For the $Li_3CuB_3O_7$ structure these correspond to the 1*a* sites. Gray polyhedra represent CuO_4 squares.

that in simple lithium borates such as $Li_2B_4O_7$, where a direct jump of Li along the [001] direction is not possible and thus a vacancy mechanism is operative.[33] Unfortunately, our XRD data are by far insufficient to verify a similar mechanism in $Li_3CuB_3O_7$ via a refinement of Li positions at high temperatures. Neutron diffraction experiments would be necessary for this purpose.

In $Li_2Cu_9B_{12}O_{28}$, an enhanced ionic conductivity and a possibility for the insertion of lithium atoms could be expected as well. The lithium atoms occupy large cavities built up of tetraborate B_4O_9 units and CuO_4 squares. Additional Li atoms could occupy the 1*h* (0.5, 0.5, 0.5) sites. The average Cu−O distance of 1.97 Å in the CuO_4 squares around the cavities would match for copper(I) in the case of lithium intercalation. The copper vacancies in the Cu(6) positions, which are corner-sharing with LiO_5 polyhedra, should also benefit a vacancy mechanism for lithium transport.

Although the crystal structure of $Li_6CuB_4O_{10}$ exhibits small channels along the *a* axis (Figure 5), the insertion of additional lithium atoms on the 1*c* sites in the middle of the channels while preserving the structure is rather unlikely because of too long Li−O bond lengths of 2.32 and 2.78 Å for the inserted lithium. However, this 1*c* site could be involved in lithium transport as a transition state.

$Li_8Cu_7B_{14}O_{32}$ does not have any visible channels in the structure, whereas the change in the orientation of layered segments from BO_3 triangles to CuO_4 squares along the *a* axis (Figure 7b) would further impede a hopping mechanism of Li migration in the structure. Therefore, this compound is probably not suitable for Li intercalation.

Although the crystal structures of lithium copper borates seem to be influenced by the strong Jahn−Teller distortion of Cu^{2+}, the oxidation or reduction of copper would not necessarily destroy these complex frameworks because both Cu^+ and Cu^{3+} may support the square-planar oxygen coordination. We believe that at least two new copper borates reported in this work may be promising materials for the intercalation of lithium. Their further investigation is highly desirable.

2. Magnetic Properties. Presently, only $Li_3CuB_3O_7$ and $Li_8Cu_7B_{14}O_{32}$ could be prepared as bulk powder samples without magnetic impurities. In the following, we report the

dx.doi.org/10.1021/ic4015724 | *Inorg. Chem.* 2013, 52, 13974−13983

magnetic properties and a brief microscopic analysis of these novel Cu^{2+} borates.

2.1. $Li_3CuB_3O_7$. The magnetic susceptibility of $Li_3CuB_3O_7$ shows a broad maximum around 220 K indicative of short-range antiferromagnetic order. At low temperatures, the susceptibility becomes negative and keeps decreasing, although with a slight upturn below 50 K (Figure 9). While the presence

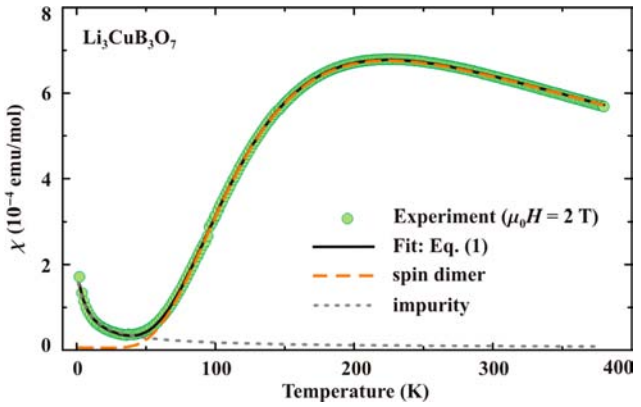

Figure 9. Magnetic susceptibility of $Li_3CuB_3O_7$ and its fit to eq 1, shown by the dark solid line. The dashed and dotted lines are the intrinsic susceptibility of the spin dimer and the Curie-like contribution of paramagnetic impurities, as given by the first and second terms of eq 1, respectively.

of Cu^{2+} ions renders $Li_3CuB_3O_7$ paramagnetic, multiple diamagnetic contributions related to the core diamagnetism, sample holder, and the $LiBO_2$ impurity phase lead to the overall diamagnetic signal at low temperatures. As the crystal structure of $Li_3CuB_3O_7$ features well-defined Cu_2O_6 dimers (Figure 1), we analyzed the experimental magnetic susceptibility using the model of an isolated spin dimer,

$$\chi = \frac{N_A g^2 \mu_B{}^2}{k_B T} \frac{1}{\exp(J/k_B T) + 3} + \frac{C}{T + \theta} + \chi_0 \qquad (1)$$

where the first term is the susceptibility of an isolated spin dimer with intradimer coupling J, the second term is the Curie–Weiss contribution of defects or impurities responsible for the low-temperature upturn, and χ_0 is the temperature-independent diamagnetic contribution. Using Avogadro's number (N_A), the Bohr magneton (μ_B), and Boltzmann's constant (k_B), we arrived at an excellent fit with J = 361.9(2) K, g = 1.79(1), C = 1.4(1) × 10^{-3} emu K/mol, χ_0 = 0, and θ = 7.2(4) K. Although the amount of the paramagnetic impurity is as low as 0.4% (w/w), the respective contribution is clearly visible as the low-temperature upturn in the susceptibility, because at low temperatures the intrinsic susceptibility of $Li_3CuB_3O_7$ is vanishingly small.

In eq 1, g stands for the g factor, which is typically above 2.0 in Cu^{2+} compounds.[34−36] Our fitted value was below 2.0, though. This discrepancy can be attributed to interdimer interactions that modify the first term of eq 1[34] and/or to diamagnetic contributions that merely scale this term down. To elucidate the role of the interdimer interactions, we calculated individual magnetic couplings within DFT. A qualitative scenario can be obtained directly from the LDA band structure, where two bands of Cu $3d_{x^2-y^2}$ origin are found right below the Fermi level and about 0.4 eV above the Fermi level (Figure 9). Here the x and y axes are directed toward neighboring Cu atoms, and x^2-y^2 is the highest crystal-field level of Cu^{2+}. The LDA band gap is somewhat small considering the pale-blue color of $Li_3CuB_3O_7$. However, underestimated band gaps are a typical shortcoming of the LDA[22−24] due to the missing part of electronic correlations in the Cu 3d shell.

An isolated dimer would manifest itself by two flat bands separated by 2t, where t measures the intradimer interaction (electron hopping between the sites of the dimer). The calculated LDA bands (Figure 10) are close to this ultimate

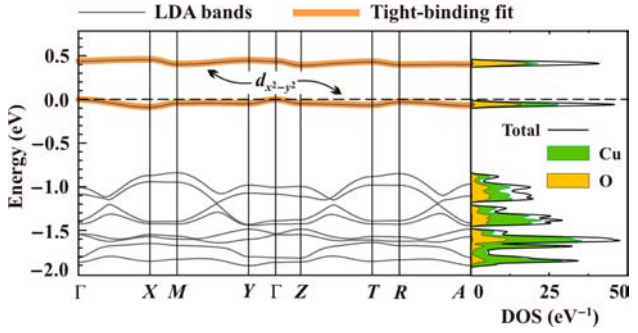

Figure 10. (left) LDA band structure of $Li_3CuB_3O_7$ showing the two $d_{x^2-y^2}$ bands arising from weakly coupled Cu_2O_6 dimers. (right) Electronic density of states, with Cu and O contributions marked by different colors. The contribution of B orbitals is negligible in this energy range.

scenario, although the weak dispersion evidences nonzero interdimer couplings. When these couplings were taken into account, we obtained t = 0.235 eV for the intradimer hopping and t' = −0.016 eV for the leading interdimer interaction. Since $J \sim t^2$,[22−24] the J'/J ratio was well below 0.01, so the interdimer couplings should have little or no effect on the magnetic behavior. A quantitative estimate of J could be obtained from LSDA+U calculations, which yielded J = 343 K, in good agreement with the experimental value of 362 K.

Our DFT results confirmed that the model of isolated spin dimers is appropriate for the description of $Li_3CuB_3O_7$. The low g value obtained from the susceptibility fit is therefore a mere consequence of diamagnetic impurities that reduce the intrinsic signal of $Li_3CuB_3O_7$, thus leading to an underestimation of the g value (note that in eq 1, g is a simple scaling factor).

The strong antiferromagnetic exchange within the Cu_2O_6 dimer is somewhat unexpected, because this coupling geometry entails Cu–O–Cu bridging angles close to 90°. Although the Goodenough–Kanamori–Anderson rules prescribe ferromagnetic exchange for bridging angles close to 90°, even a minor deviation toward larger angles may result in an overall antiferromagnetic coupling,[37] as seen in $SrCu_2(BO_3)_2$ with the bridging angle of about 98.0° ($J \approx$ 85 K).[38] Larger bridging angles lead to larger antiferromagnetic couplings, as in α-$Cu_2As_2O_7$ ($J \approx$ 164 K, Cu–O–Cu angle of 101.7°)[34] and $Cu_3AsO_4(OH)_3$ ($J \approx$ 290 K K, Cu–O–Cu angle of 101.9°).[39] Nevertheless, the J value of 362 K in $Li_3CuB_3O_7$ is clearly exceptional, especially considering the Cu–O–Cu angle of only 100.4° in this Cu^{2+} borate.

This comparison suggests that borate anions are more efficient than arsenate anions in mediating the Cu–O–Cu superexchange. The same trend is seen in $CdCu_2(BO_3)_2$, where $J \approx$ 180 K (i.e., as large as in α-$Cu_2As_2O_7$) despite the bridging angle of only 98.2°.[40] However, $SrCu_2(BO_3)_2$ with a similar

dx.doi.org/10.1021/ic4015724 | Inorg. Chem. 2013, 52, 13974−13983

bridging angle of about 98.0° features a weaker exchange of $J \approx 85$ K.[38] Thus, the magnetic exchange is highly sensitive to details of the atomic arrangement. The values of the bridging angles, as considered in the Goodenough–Kanamori–Anderson rules, provide only a rough picture. For a given bridging angle, the coupling may vary within 100–200 K depending on the structure of the Cu_2O_6 dimer [e.g., whether it is flat as in $CdCu_2(BO_3)_2$ or bent as in $SrCu_2(BO_3)_2$] and surrounding anions (e.g., BO_3 in borates or AsO_4 in arsenates).

In contrast to other Cu^{2+} compounds, long-range superexchange pathways play a little role in the magnetism of $Li_3CuB_3O_7$. The leading interdimer exchange connects neighboring dimers along [110] and involves a long Cu–O–O–Cu pathway with two oxygen atoms separated for 4.5 Å by a Li cation. We did not find any appreciable superexchange involving BO_3 triangles because these triangles simply encompass the dimer without linking neighboring dimers to each other. By contrast, when nonmagnetic polyhedra link the Cu_2O_6 dimers, sizable Cu–O–O–Cu super-superexchange couplings emerge, as in $CuWO_4$ and the isostructural $CuMoO_4$-III polymorph.[41,42]

2.2. $Li_8Cu_7B_{14}O_{32}$. Above 100 K, the magnetic susceptibility of $Li_8Cu_7B_{14}O_{32}$ shows only a weak temperature dependence with a very broad bend around 150 K (Figure 11). Below 100 K, the susceptibility sharply increases. Although the complex crystal structure of this compound prevented a detailed microscopic analysis, a simple phenomenological interpretation can be given using the inverse susceptibility $1/\chi$. The two linear parts of the curve yielded $\mu_{eff} = 0.6\mu_B/Cu^{2+}$, $\theta = -0.7$ K below 50 K and $\mu_{eff} = 1.43\mu_B/Cu^{2+}$, $\theta = -224$ K above 200 K. The high value of θ at high temperatures indicates strong antiferromagnetic coupling between the Cu^{2+} ions. At low temperatures, θ is close to zero, which shows that the antiferromagnetic couplings eventually split the system into weakly interacting magnetic moieties that bear a nonzero magnetic moment manifesting itself by a Curie–Weiss-like magnetic behavior (linear region in $1/\chi$).

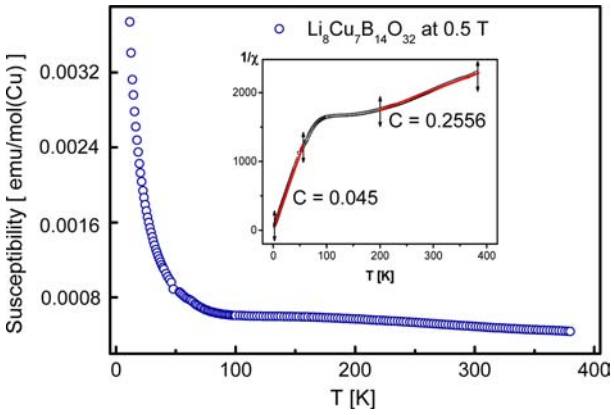

Figure 11. Magnetic susceptibility (χ) of $Li_8Cu_7B_{14}O_{32}$ and (inset) the inverse susceptibility ($1/\chi$) vs temperature.

The low-temperature effective moment is $1.59\mu_B$/f.u. and roughly corresponds to one unpaired electron per formula unit (f.u.), which should yield $\mu_{eff} = 1.73\mu_B$/f.u. for a spin-only contribution. This low-temperature regime implies that six out of seven Cu^{2+} ions are coupled antiferromagnetically, while the remaining Cu^{2+} spin is idle. An identification of these antiferromagnetically coupled and idle spins among the Cu(1)–Cu(4) crystallographic sites is, however, not possible. It would require a careful evaluation of individual exchange couplings that lies beyond the scope of the present study.

The high-temperature Curie–Weiss regime shows that the magnetic couplings in $Li_8Cu_7B_{14}O_{32}$ are predominantly antiferromagnetic. However, the effective moment, which is somewhat lower than $1.73\mu_B/Cu^{2+}$, reflects residual interactions present up to at least 380 K. Overall, the spin system of $Li_8Cu_7B_{14}O_{32}$ is very complex. It combines Cu_2O_6 dimers, Cu_3O_8 trimers, and individual CuO_4 plaquettes that may be attached to Cu_3O_8 trimers when the Cu(3) site is taken by Cu^{2+} or isolated when the Cu(3) site is occupied by Li^+ (Figure 7). This coexistence of different magnetic units is reminiscent of intricate and still poorly understood Cu^{2+} magnets such as $Na_2Cu_5Si_4O_{14}$.[43,44] We hope that advanced computational studies will be capable of elucidating magnetic models of these intricate compounds.

CONCLUSIONS

Three new centrosymmetric and one non-centrosymmetric lithium copper borates were identified in the Li_2O–CuO–B_2O_3 system after high-temperature syntheses in air. In all of the compounds, boron atoms form BO_3 triangles that share corners and edges with other polyhedra. Despite the different stoichiometries, the obtained borates show certain similarities in the hierarchical borate classification that is generally used in borate chemistry.[45] This classification is based on the topological character of fundamental building blocks as finite clusters $[B_nO_m]$ with $n \leq 6$ and the structural units.[45] Only a simple sequence of clusters containing corner-sharing BO_3 triangles without complex polymerization was observed for all of the new lithium copper borates. For example, a polyborate anion consisting of several corner-sharing BO_3 triangles can be described as 3Δ:ΔΔΔ in $Li_3CuB_3O_7$, as 4Δ:ΔΔΔΔ and 2Δ:ΔΔ in $Li_2Cu_9B_{12}O_{28}$, as 2Δ:ΔΔ in $Li_6CuB_4O_{10}$, and as 5Δ:ΔΔΔΔΔ and 2Δ:ΔΔ in $Li_8Cu_7B_{14}O_{32}$. The shortest unit cell dimension in all of the obtained borates corresponds to the nearest Cu–Cu interatomic distance of about 3.3 Å. Copper atoms form different coordination polyhedra, including squares, square pyramids, and distorted octahedra. Strongly anisotropic thermal expansion behavior was found for $Li_3CuB_3O_7$, which exhibited a much larger expansion along the *a* axis between planes in which the Cu_2O_6 dimers of edge-sharing CuO_4 squares are located. Because of the presence of structural channels, $Li_3CuB_3O_7$ and $Li_8Cu_7B_{14}O_{32}$ can be promising materials for lithium insertion and should possess high ionic conductivity. High ionic conductivity is also expected for $Li_6CuB_4O_{10}$. The magnetism of $Li_3CuB_3O_7$ is well-understood in terms of the model of isolated spin dimers. The intradimer coupling ($J \approx 360$ K) is remarkably large for the Cu_2O_6 structural dimer. $Li_8Cu_7B_{14}O_{32}$ shows complex magnetic behavior with at least two different linear regimes in the inverse susceptibility $1/\chi$.

ASSOCIATED CONTENT

Supporting Information

Atomic coordinates and equivalent isotropic displacement parameters (Tables A–D) and interatomic distances (Tables E–H) for the reported compounds. This material is available free of charge via the Internet at http://pubs.acs.org.

AUTHOR INFORMATION

Corresponding Author

*E-mail: Daria.Mikhailova@cpfs.mpg.de.

Notes

The authors declare no competing financial interest.

ACKNOWLEDGMENTS

The authors are indebted to J.-C. Jaud (Institute for Materials Science, Darmstadt University of Technology, Darmstadt, Germany) for performing high-temperature PXRD measurements. A.A.T. was partially supported by the Alexander von Humboldt Foundation and the MTT77 Mobilitas Grant of the ESF.

REFERENCES

(1) Pan, S.; Smit, J. P.; Watkins, B.; Marvel, M. R.; Stern, C. L.; Poeppelmeier, K. R. *J. Am. Chem. Soc.* **2006**, *128*, 1163−1164.
(2) Khalil, M. M. I. *Appl. Phys. A: Mater. Sci. Process.* **2007**, *86*, 505−514.
(3) Kageyama, H.; Yoshimura, K.; Stern, R.; Mushnikov, N. V.; Onizuka, K.; Kato, M.; Kosuge, K.; Slichter, C. P.; Goto, T.; Ueda, Y. *Phys. Rev. Lett.* **1999**, *82*, 3168−3171.
(4) Saito, M.; Ishikawa, K.; Konno, S.; Taniguchi, K.; Arima, T. *Nat. Mater.* **2009**, *8*, 634−638.
(5) Liu, J.; Wen, S.; Zou, X.; Zuo, F.; Beran, G. J. O.; Feng, P. *J. Mater. Chem. A* **2013**, *1*, 1553−1556.
(6) Débart, A.; Revel, B.; Dupont, L.; Montagne, L.; Leriche, J.-B.; Touboul, M.; Tarascon, J.-M. *Chem. Mater.* **2003**, *15*, 3683−3691.
(7) Parzych, G.; Mikhailova, D.; Oswald, S.; Eckert, J.; Ehrenberg, H. *J. Electrochem. Soc.* **2011**, *158*, A898−A904.
(8) Pardo, J.; Martinez-Ripoll, M.; García-Blanco, S. *Acta Crystallogr.* **1974**, *B30*, 37−40.
(9) Behm, H. *Acta Crystallogr.* **1982**, *B38*, 2781−2784.
(10) Kuratieva, N.; Mikhailova, D.; Ehrenberg, H. *Acta Crystallogr.* **2009**, *C65*, i85−i86.
(11) Yang, T.; Li, G.; You, L.; Ju, J.; Liao, F.; Lin, J. *Chem. Commun.* **2005**, 4225−4227.
(12) Marinez-Ripoll, M.; Martínez-Carrera, S.; García-Blanco, S. *Acta Crystallogr.* **1971**, *B27*, 677−681.
(13) Knyrim, J. S.; Friedrichs, J.; Neumair, S.; Roeßner, F.; Floredo, Y.; Jakob, S.; Johrendt, D.; Glaum, R.; Huppertz, H. *Solid State Sci.* **2008**, *10*, 168−176.
(14) Abdullaev, G. K.; Riza-Zade, P. F.; Mamedov, Kh. S. *Russ. J. Inorg. Chem.* **1982**, *27*, 1837−1841.
(15) Sparta, K. Structural Investigation of Quaternary Copper Oxides with Low-Dimensional Magnetic Properties. Ph.D. Thesis, Institut für Kristallographie of the RWTH-Aachen, Aachen, Germany, 2003.
(16) Sheldrick, G. M. *Acta Crystallogr.* **2008**, *A64*, 112−122.
(17) *X-STEP32*; Stoe & Cie GmbH: Darmstadt, Germany, 2000.
(18) *CrysAlis Red, CCD Data Reduction GUI*, version 1.171.26; Oxford Diffraction Poland: Wroclaw, Poland, 2005.
(19) (a) *APEX2*, version 1.08; Bruker AXS: Madison, WI, 2004. (b) *SAINT*, version 7.03; Bruker AXS: Madison, WI, 2004. (c) *SADABS*, version 2.11; Bruker AXS: Madison, WI, 2004.
(20) Koepernik, K.; Eschrig, H. *Phys. Rev. B* **1999**, *59*, 1743−1757.
(21) Perdew, J. P.; Wang, Y. *Phys. Rev. B* **1992**, *45*, 13244−13249.
(22) Tsirlin, A. A.; Janson, O.; Rosner, H. *Phys. Rev. B* **2010**, *82*, No. 144416.
(23) Tsirlin, A. A.; Abakumov, A. M.; Ritter, C.; Rosner, H. *Phys. Rev. B* **2012**, *86*, No. 064440.
(24) Lebernegg, S.; Tsirlin, A. A.; Janson, O.; Nath, R.; Sichelschmidt, J.; Skourski, Yu.; Amthauer, G.; Rosner, H. *Phys. Rev. B* **2011**, *84*, No. 174436.
(25) Bazarova, Zh. G.; Nepomnyashchikh, A. I.; Kozlov, A. A.; Bogdan-Kurilo, V. D.; Bazarov, B. G.; Subanakov, A. K.; Kurbatov, R. V. *Russ. J. Inorg. Chem.* **2007**, *52*, 1971−1973.
(26) Kirfel, A.; Will, G.; Stewart, R. F. *Acta Crystallogr.* **1983**, *B39*, 175−185.
(27) Buludov, N.; Karaev, Z.; Abdullaev, G. *Russ. J. Inorg. Chem. (Engl. Transl.)* **1986**, *31*, 1215.
(28) Brown, I. D.; Altermatt, D. *Acta Crystallogr.* **1985**, *B41*, 244−247.
(29) Brown, I. D. *Acta Crystallogr.* **1992**, *B48*, 553−572.
(30) Rao, G. H.; Bärner, K.; Brown, I. D. *J. Phys.: Condens. Matter* **1998**, *10*, L757−L763.
(31) Shannon, R. D. *Acta Crystallogr.* **1976**, *A32*, 751−762.
(32) Spek, A. L. *J. Appl. Crystallogr.* **2003**, *36*, 7−13.
(33) Islam, M. M.; Bredow, T.; Heitjans, P. *J. Phys.: Condens. Matter* **2012**, *24*, No. 203201.
(34) Arango, Y. C.; Vavilova, E.; Abdel-Hafiez, M.; Janson, O.; Tsirlin, A. A.; Rosner, H.; Drechsler, S.-L.; Weil, M.; Nénert, G.; Klingeler, R.; Volkova, O.; Vasiliev, A.; Kataev, V.; Büchner, B. *Phys. Rev. B* **2011**, *84*, No. 134430.
(35) Janson, O.; Tsirlin, A. A.; Sichelschmidt, J.; Skourski, Y.; Weickert, F.; Rosner, H. *Phys. Rev. B* **2011**, *83*, No. 094435.
(36) Umegaki, I.; Tanaka, H.; Ono, T.; Uekusa, H.; Nojiri, H. *Phys. Rev. B* **2009**, *79*, No. 184401.
(37) Rocquefelte, X.; Schwarz, K.; Blaha, P. *Sci. Rep.* **2012**, *2*, 759.
(38) Miyahara, S.; Ueda, K. *J. Phys.: Condens. Matter* **2003**, *15*, R327−R366.
(39) Lebernegg, S.; Tsirlin, A. A.; Janson, O.; Rosner, H. 2013, arXiv:1304.0964. arXiv.org e-Print archive. http://arxiv.org/abs/1304.0964 (accessed Nov 18, 2013).
(40) Janson, O.; Rousochatzakis, I.; Tsirlin, A. A.; Richter, J.; Skourski, Y.; Rosner, H. *Phys. Rev. B* **2012**, *85*, No. 064404.
(41) Koo, H.-J.; Whangbo, M.-H. *Inorg. Chem.* **2001**, *40*, 2161−2169.
(42) Schwarz, B. C.; Ehrenberg, H.; Weitzel, H.; Fuess, H. *Inorg. Chem.* **2007**, *46*, 378−380.
(43) Moreira dos Santos, A.; Brandão, P.; Fitch, A.; Reis, M. S.; Amaral, V. S.; Rocha, J. *J. Solid State Chem.* **2007**, *180*, 16−21.
(44) Reis, M. S.; Moreira dos Santos, A.; Amaral, V. S.; Brandão, P.; Rocha, J. *Phys. Rev. B* **2006**, *73*, No. 214415.
(45) Burns, P. C.; Grice, J. D.; Hawthorne, F. C. *Can. Mineral.* **1995**, *33*, 1131−1151.